

Isolated highly localized bands in YbI₂ monolayer caused by 4*f* orbitals

San-Dong Guo

Department of Physics, School of Sciences, China University of Mining and Technology, Xuzhou 221116, Jiangsu, China

The novel electronic structures can induce unique physical properties in two-dimensional (2D) materials. In this work, we report isolated highly localized bands in YbI₂ monolayer by the first-principle calculations within generalized gradient approximation (GGA) plus spin-orbit coupling (SOC). It is found that YbI₂ monolayer is an indirect-gap semiconductor using both GGA and GGA+SOC. The calculations reveal that Yb-4*f* orbitals constitute isolated highly localized bands below the Fermi level at the absence of SOC, and the bands are split into the $j = 7/2$ and $j = 5/2$ states with SOC. The isolated highly localized bands can lead to very large Seebeck coefficient and very low electrical conductivity in p-type doping by producing very large effective mass of the carrier. It is proved that isolated highly localized bands have very strong stability against strain, which is very important for practical application. When the onsite Coulomb interaction is added to the Yb-4*f* orbitals, isolated highly localized bands persist, and only their relative positions in the gap change. These findings open a new window to search for novel electronic structures in 2D materials.

PACS numbers: 71.20.-b, 73.22.-f, 72.20.-i, 74.62.F

Email:sandongyuwang@163.com

Keywords: Monolayer; Spin-orbit coupling; Novel electronic structures; Strain

I. INTRODUCTION

Since the discovery of graphene¹, 2D materials have attracted enormous research interest in electronic, optical, topological and thermal properties. A large amount of 2D materials have been predicted theoretically, or achieved experimentally, such as transition metal dichalcogenide (TMD), group-VA, group IV-VI and group-IV monolayers²⁻⁶. Graphene has a peculiar electronic structure with the dispersion relation being linear around the Fermi level, and the related electrons and holes need to be described by the Dirac equation¹. Compared with the gapless graphene, MoS₂ as a representative semiconducting TMD monolayer has triggered a new wave of research in TMD monolayers due to potential application for novel ultrathin and flexible devices^{7,8}. Recently, Janus monolayer MoSSe has been experimentally synthesized by replacing the top S atomic layer of MoS₂ with Se atoms⁹, which provides more possibilities for more extensive nanoelectronic and optoelectronic applications. Phosphorene, possessing novel high carrier mobility and intrinsically large fundamental direct band gap, has great prospective for its applications in field-effect transistors and photo-transistors^{10,11}. Experimentally, the 2D Dirac nodal line fermions has been reported in monolayer Cu₂Si, which provides a platform to study the novel physical properties in 2D Dirac materials¹². Thermal transports of 2D materials have been widely investigated, including external perturbation like strain, substrate and clustering¹³.

Searching for other peculiar electronic structure, like isolated highly localized bands, would be of great significance to the design and development of nano-devices. Recently, the plentiful 2D materials are predicted from high-throughput computational exfoliation of experimentally known compounds¹⁴. Among them, YbI₂ monolayer with 4*f* electrons is predicted, which is interesting to investigate its electronic structure due to localized 4*f*

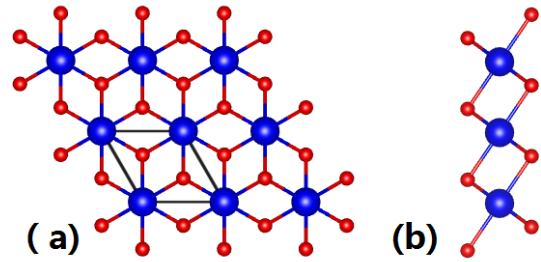


FIG. 1. (Color online) The schematic crystal structure of YbI₂ monolayer. The blue balls represent Yb atoms, and the red balls for I atoms.

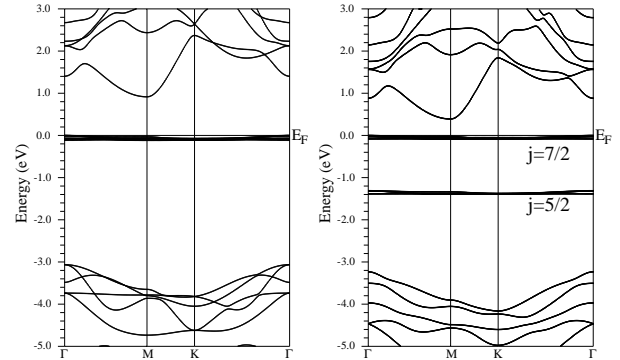


FIG. 2. The energy band structures of YbI₂ monolayer using GGA (Left) and GGA+SOC (Right).

orbitals. In this work, the electronic structures of YbI₂ monolayer are studied by first-principles calculations. It is found that there are some isolated highly localized bands with Yb-4*f* character in a very large gap. The SOC can split the 4*f* bands into $j = 7/2$ and $j = 5/2$ states, and the splitting gap is up to about 1.22 eV. In p-type doping, the very large Seebeck coefficient and very low electrical conductivity can be found due to very large

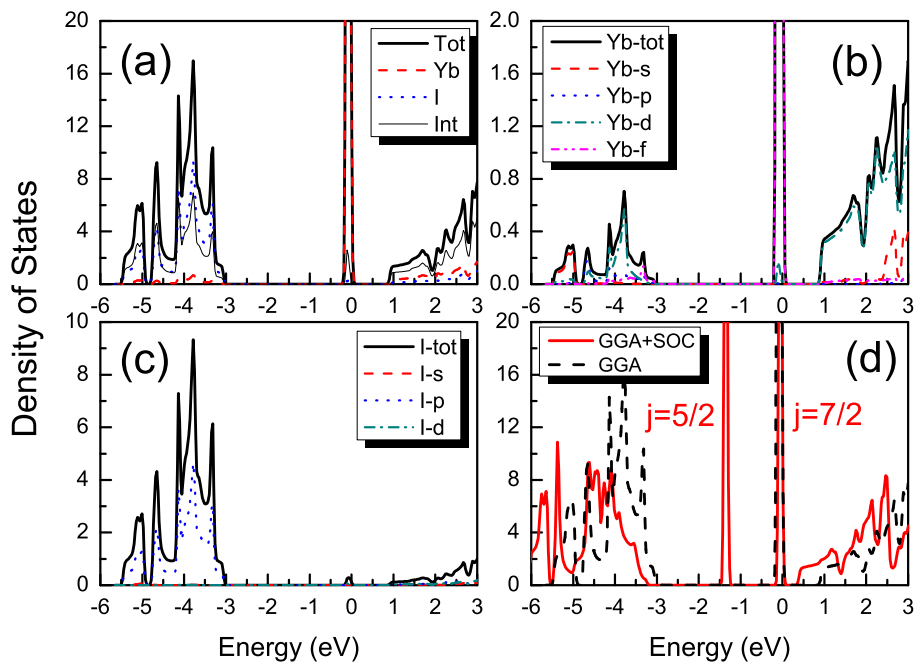


FIG. 3. (a,b,c) the total and projected DOS of YbI₂ monolayer using GGA; (d) the total DOS using GGA and GGA+SOC.

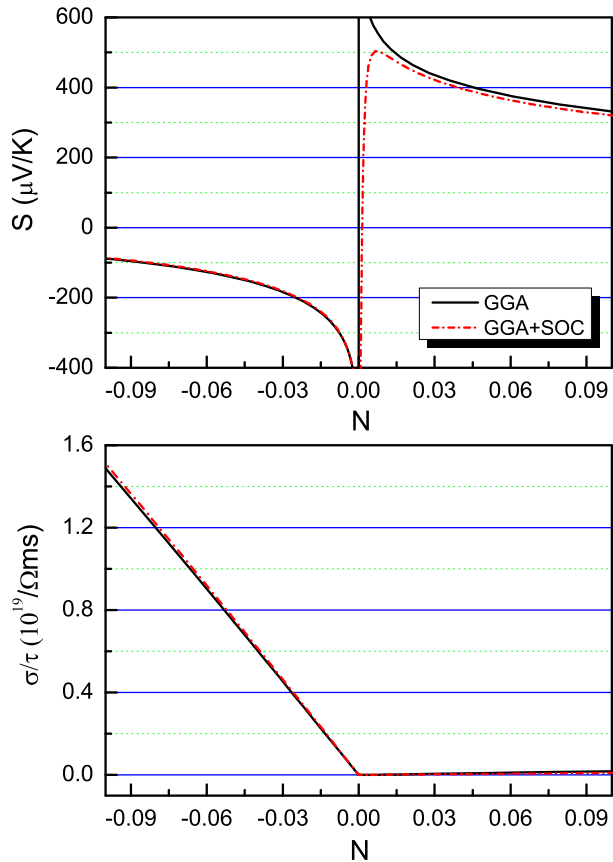


FIG. 4. At 300 K, the transport coefficients of YbI₂ monolayer as a function of doping level (N) using GGA and GGA+SOC: Seebeck coefficient S and electrical conductivity with respect to scattering time σ/τ .

effective mass of the p-type carrier caused by the isolated highly localized bands. Calculated results show that isolated highly localized bands are very stable against strain, and the electron correlation effects only change the relative positions of highly localized bands in the gap.

II. COMPUTATIONAL DETAIL

Within the density functional theory (DFT)¹⁵, we use a full-potential linearized augmented-plane-waves method to investigate electronic structures of YbI₂ monolayer, as implemented in the WIEN2k code¹⁶. The popular GGA of Perdew, Burke and Ernzerhof (GGA-PBE)¹⁷ is used as the exchange-correlation potential, and the internal atomic positions are optimized with a force standard of 2 mRy/a.u.. Due to containing heavy element Yb, the SOC was included self-consistently^{18–21}. To attain reliable results, we use $30 \times 30 \times 1$ k-meshes in the first Brillouin zone (BZ) for the self-consistent calculation with harmonic expansion up to $l_{\max} = 10$ and $R_{\text{mt}} * k_{\max} = 8$. The self-consistent calculations are considered to be converged when the integration of the absolute charge-density difference between the input and output electron density is less than $0.0001|e|$ per formula unit, where e is the electron charge. Based on calculated energy band structures, the Seebeck coefficient and electrical conductivity of YbI₂ are performed through solving Boltzmann transport equations within the constant scattering time approximation (CSTA), as implemented in BoltzTrap software²². To achieve the convergence results, the parameter LPFAC is set to 40, and $100 \times 100 \times 1$ k-meshes in the first BZ is used for the energy band cal-

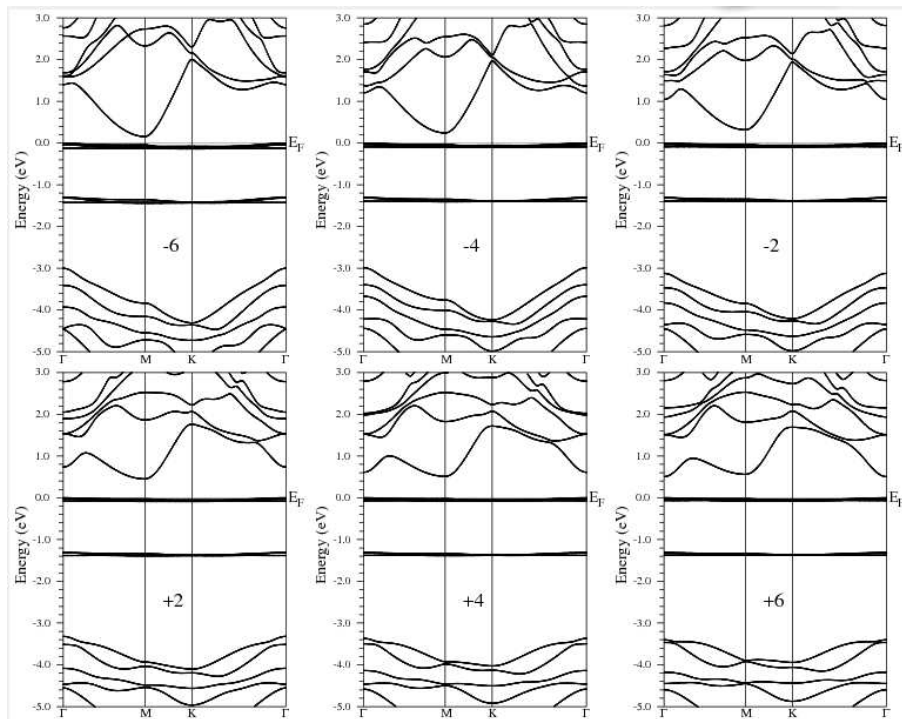


FIG. 5. (Color online) The energy band structures of YbI_2 monolayer with ε changing from -6% to 6% using GGA+SOC.

ulation.

III. MAIN CALCULATED RESULTS AND ANALYSIS

Figure 1 shows the structure of YbI_2 monolayer, containing three atomic sublayers with Yb layer sandwiched I layers. The similar structure can also be found in TMD monolayer²³, such as ZrS_2 and PtSe_2 monolayers with 1T phase. However, it is different from the MoS_2 as a representative TMD monolayer with 2H phase. The unit cell of YbI_2 monolayer is built with the vacuum region of more than 18 Å to avoid spurious interaction between neighboring layers. The optimized lattice constants a (b) using GGA is 4.46 Å with Yb and I atoms occupying the (0, 0, 0) and (1/3, 2/3, 0.922) positions, respectively. The Yb-I bond length is 3.14 Å, and I-Yb-I bond angle for 89.265° (90.735°), and the thicknesses of YbI_2 monolayer for 3.58 Å.

The calculated energy band structures of YbI_2 monolayer are shown in Figure 2 with GGA and GGA+SOC, and the related density of states (DOS) are plotted in Figure 3. Without SOC, fourteen highly localized bands with Yb-4*f* character are observed near the Fermi level, and the bandwidth is only 0.118 eV. When including SOC, the 4*f* bands are split into the $j = 7/2$ and $j = 5/2$ states, producing a gap of 1.218 eV. Similar splitting can also be found in YbB_6 by SOC²⁴. The $j = 7/2$ states are near the Fermi level with bandwidth 0.092 eV, and $j = 5/2$ states are -1.309 eV below the Fermi level with

bandwidth 0.086 eV. Both using GGA and GGA+SOC, the valence band maximum (VBM) is at Γ point, and the conduction band minimum (CBM) at M point. The GGA and GGA+SOC gap is 0.916 eV and 0.390 eV, respectively, and the gap reduce caused by SOC is 0.526 eV. The bands from -5.5 to -3.0 eV are mainly composed of I-p character states, slightly hybridized with Yb-d/s ones. The hybridized Yb-d and I states are observed in the conduction bands. When considering SOC, it is found that both conduction bands and valence bands below localized states move toward lower energy compared with ones using GGA.

The electronic transport coefficients of TMD monolayers have been widely investigated in theory^{25–27}. It is natural to ask what effects on transport coefficients can be induced by highly localized bands. Based on CSTA Boltzmann theory, the Seebeck coefficient S and electrical conductivity σ/τ are performed within rigid band approach. It is noted that the calculated σ/τ depends on τ , while S is independent of τ . The n(p)-type doping effects can be simulated by simply moving the Fermi level into conduction (valence) bands, namely electron (hole) doping. The room temperature S and σ/τ of YbI_2 as a function of doping level (N) using GGA and GGA+SOC are plotted in Figure 4. In low p-type doping, a detrimental influence on S caused by SOC can be observed, while a neglectful effect on S (absolute value) in n-type or high p-type doping can be found. For σ/τ , the SOC has little effect in both n- and p-type doping. It is clearly seen that the p-type S is larger than 300 $\mu\text{V}/\text{K}$ with doping level being up to 0.1 hole/per unit cell. However, for n-type

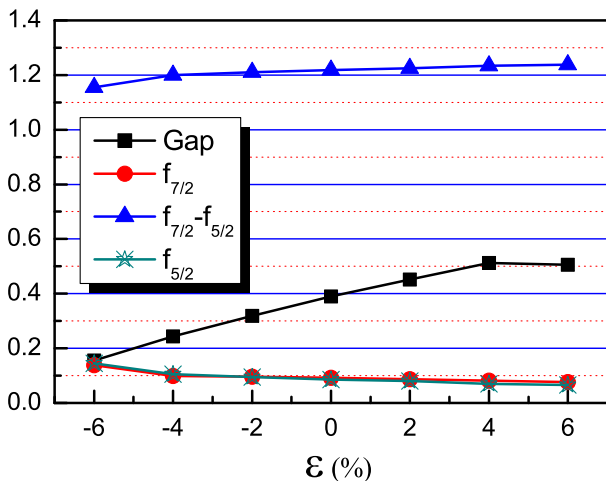


FIG. 6. (Color online) The energy band gap (Gap), the gap between the $j = 7/2$ and $j = 5/2$ states ($f_{7/2}-f_{5/2}$) and the widths of the $j = 7/2$ and $j = 5/2$ states ($f_{7/2}$ and $f_{5/2}$) (unit: eV) as a function of ϵ .

doping, the S can reach 300 $\mu\text{V}/\text{K}$, only below doping level of 0.008 electron/per unit cell. It is also found that the σ/τ is very close to zero in p-type doping. These results are because the S is proportional to the effective mass of the carrier, while σ is inversely proportional to one. Therefore, highly localized bands can induce very large S and very low σ by producing very large effective mass of the carrier. A similar effect can be found in hole-doped PbTe or PbSe^{28,29}, and the flat-band (localized bands) can be observed below their gaps.

During the fabrication process, 2D materials will commonly have residual strain. Next, we investigate the stability of highly localized bands again biaxial strain. The strain effects on the energy band structures and transport properties of TMD monolayers have been widely investigated^{26,27,30,31}. The $\epsilon = (a - a_0)/a_0$ is defined to simulate biaxial strain, in which a_0 is the unstrained lattice constant. The $\epsilon < (>) 0$ means compressive (tensile) strain. The related energy band structures of YbI₂ monolayer are shown in Figure 5 using GGA+SOC, with strain from -6% to 6%. In considered strain range, compressive strain can reduce the numbers of conduction band extrema (CBE) from two to one, while tensile strain can change relative position of two CBE. For example, at 6% strain, the CBM changes from M to Γ point, which means that tensile strain can induce conduction bands convergence between 4% and 6% strain, producing very large n-type S. Similar phenomenon caused by strain can also be found in TMD monolayers^{26,27,31}. The energy band gap, the gap between the $j = 7/2$ and $j = 5/2$ states and the widths of the $j = 7/2$ and $j = 5/2$ states as a function of ϵ are plotted in Figure 6. With increasing strain, the energy band gap increases from -6% to 4% strain, and then slightly reduces at 6% strain. It is clearly seen that the gap between the $j = 7/2$ and $j = 5/2$ states and the widths of the $j = 7/2$ and $j = 5/2$ states have very minor

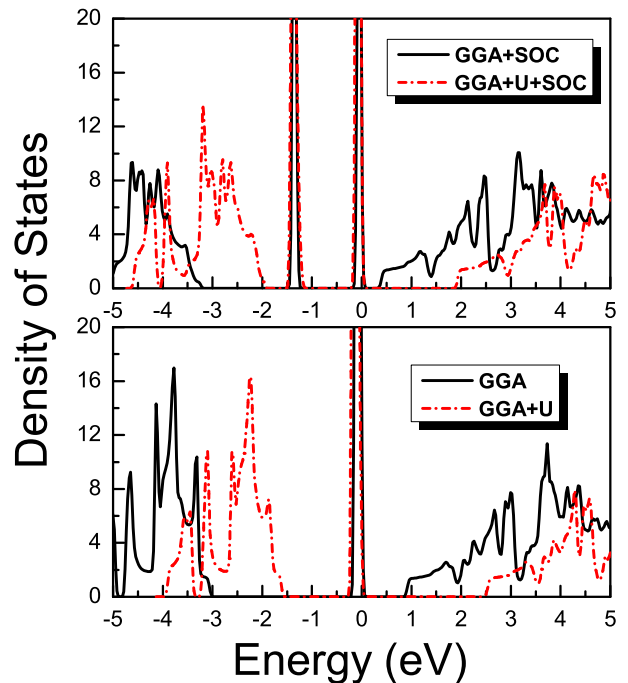


FIG. 7. The DOS of YbI₂ monolayer using GGA+SOC, GGA+U+SOC, GGA and GGA+U.

changes from -4% to 6% strain, and the change is only 0.038 eV, 0.023 eV and 0.039 eV, respectively. So, the highly localized bands have very strong stability again strain.

IV. DISCUSSIONS AND CONCLUSION

To account for 4f electron correlation effects, the on-site Coulomb interaction is included, and the Coulomb potential U_{eff} for the Yb-4f orbitals is chosen to be 5 eV. The DOS of YbI₂ using GGA+SOC, GGA+U+SOC, GGA and GGA+U are shown in Figure 7. Calculated results show that the isolated highly localized bands still exists, and only they move to lower energies, which leads to increased energy band gap. When including onsite Coulomb interaction, the GGA gap changes from 0.92 eV to 2.53 eV, and GGA+SOC gap from 0.39 eV to 1.94 eV. However, the gap between the $j = 7/2$ and $j = 5/2$ states hardly changes. In fact, as U is increased, highly localized bands gradually move to lower energies. When U is large enough, the $j = 5/2$ states firstly cross with I-p states, and then the $j = 7/2$ states also cross.

In summary, we investigate electronic structures of YbI₂ monolayer, based mainly on the reliable first-principle calculations. Calculated results show that YbI₂ monolayer is a indirect-gap semiconductor using GGA+SOC, GGA+U+SOC, GGA and GGA+U, and the isolated highly localized bands with Yb-4f character are observed in a very large gap of up to about 4 eV. With the inclusion of SOC, the 4f bands are split into

the $j = 7/2$ and $j = 5/2$ states. The isolated highly localized bands can induce very large effective mass of the p-type carrier, and then leads to very large Seebeck coefficient and very low electrical conductivity in p-type doping. Calculated results show that strain can tune the strength of conduction bands convergence by changing relative position of CBE. However, the strain has little effects on isolated highly localized bands, namely they are stable against strain. The electron correlation effects only change the relative positions of highly localized bands in the gap. Our works will motivate further experimental studies to synthesize YbI₂ monolayer, and then to detect

isolated highly localized bands.

ACKNOWLEDGMENTS

This work is supported by the National Natural Science Foundation of China (Grant No. 11404391). We are grateful to the Advanced Analysis and Computation Center of CUMT for the award of CPU hours to accomplish this work.

-
- ¹ K. S. Novoselov et al., *Science* **306**, 666 (2004).
 - ² R. X. Fei, W. B. Li, J. Li and L. Yang, *Appl. Phys. Lett.* **107**, 173104 (2015).
 - ³ J. P. Ji, X. F. Song, J. Z. Liu et al., *Nat. Commun.* **7**, 13352 (2016).
 - ⁴ S. L. Zhang M. Q. Xie, F. Y. Li, Z. Yan, Y. F. Li, E. J. Kan, W. Liu, Z. F. Chen, H. B. Zeng, *Angew. Chem.* **128**, 1698 (2016).
 - ⁵ S. Balendhran, S. Walia, H. Nili, S. Sriram and M. Bhaskaran, *small* **11**, 640 (2015).
 - ⁶ M. Chhowalla, H. S. Shin, G. Eda, L. J. Li, K. P. Loh and H. Zhang, *Nature Chemistry* **5**, 263 (2013).
 - ⁷ B. Radisavljevic, A. Radenovic, J. Brivio, V. Giacometti and A. Kis, *Nat. Nanotechnol.* **6**, 147 (2011).
 - ⁸ D. Jariwala, V. K. Sangwan, L. J. Lauhon, T. J. Marks and M. C. Hersam, *ACS Nano* **8**, 1102 (2014).
 - ⁹ A. Y. Lu, H. Y. Zhu, J. Xiao et al., *Nature Nanotechnology* **12**, 744 (2017).
 - ¹⁰ H. Liu, A. T. Neal, Z. Zhu, Z. Luo, X. Xu, D. Tomnek, and P. D. Ye, *ACS Nano* **8**, 4033 (2014).
 - ¹¹ H. O. H. Churchill and P. Jarillo-Herrero, *Nat. Nanotech.* **9**, 330 (2014).
 - ¹² B. J. Feng, B. T. Fu, S. Kasamatsu et al., *Nat. Commun.* **8**, 1007 (2017).
 - ¹³ C. Shao, X. X. Yu, N. Yang, Y. N. Yue and H. Bao, *Nanoscale Microsc. Therm.* **21**, 201 (2017).
 - ¹⁴ N. Mounet, M. Gibertini, P. Schwaller et al., *Nat. Nanotechnol.* **13**, 246 (2018).
 - ¹⁵ P. Hohenberg and W. Kohn, *Phys. Rev.* **136**, B864 (1964); W. Kohn and L. J. Sham, *Phys. Rev.* **140**, A1133 (1965).
 - ¹⁶ P. Blaha, K. Schwarz, G. K. H. Madsen, D. Kvasnicka and J. Luitz, WIEN2k, an Augmented Plane Wave + Local Orbitals Program for Calculating Crystal Properties (Karlheinz Schwarz Technische Universität Wien, Austria) 2001, ISBN 3-9501031-1-2
 - ¹⁷ J. P. Perdew, K. Burke and M. Ernzerhof, *Phys. Rev. Lett.* **77**, 3865 (1996).
 - ¹⁸ A. H. MacDonald, W. E. Pickett and D. D. Koelling, *J. Phys. C* **13**, 2675 (1980).
 - ¹⁹ D. J. Singh and L. Nordstrom, *Plane Waves, Pseudopotentials and the LAPW Method*, 2nd Edition (Springer, New York, 2006).
 - ²⁰ J. Kunes, P. Novak, R. Schmid, P. Blaha and K. Schwarz, *Phys. Rev. B* **64**, 153102 (2001).
 - ²¹ D. D. Koelling, B. N. Harmon, *J. Phys. C: Solid State Phys.* **10**, 3107 (1977).
 - ²² G. K. H. Madsen and D. J. Singh, *Comput. Phys. Commun.* **175**, 67 (2006).
 - ²³ H. L. Zhuang and R. G. Hennig, *J. Phys. Chem. C* **117**, 20440 (2013).
 - ²⁴ T. R. Chang, T. Das, P. J. Chen et al., *Phys. Rev. B* **91**, 155151 (2015).
 - ²⁵ S. D. Guo and J. L. Wang, *Semicond. Sci. Tech.* **31**, 095011 (2016).
 - ²⁶ H. Y. Lv, W. J. Lu, D. F. Shao, H. Y. Lub and Y. P. Sun, *J. Mater. Chem. C* **4**, 4538 (2016).
 - ²⁷ S. D. Guo, *J. Mater. Chem. C* **4**, 9366 (2016).
 - ²⁸ D. Parker and D. J. Singh, *Phys. Rev. B* **82**, 035204 (2010).
 - ²⁹ D. J. Singh, *Phys. Rev. B* **81**, 195217 (2010).
 - ³⁰ E. Scalise, M. Houssa, G. Pourtois, V. Afanas'ev and A. Stesmans, *Nano Res.* **5**, 43 (2012).
 - ³¹ D. Qin, X. J. Ge, G. Q. Ding, G. Y. Gao and J. T. Lv, *RSC Adv.* **7**, 47243 (2017).